Electron Irradiation and Raman Characterization of Reduced Graphene Oxide Film

Avin Gupta
Texas Academy of Math and Science
September 28, 2025

Acknowledgement of Major Assistance

This work was conducted over the 2025 summer and fall semesters at the University of North Texas in Denton, specifically in the Physics Department and in the lab of Dr. Jose Perez. I thank the university for providing me with a summer research scholarship. Additionally, I would like to acknowledge the following individuals who assisted me with the study: Dr. Jose Perez, University of North Texas; Jacob Hardin, University of North Texas; Anil Pusaidini, University of North Texas; Mahendra Subedi, University of North Texas; Thineth Hitihamilage, University of North Texas; and Franklin Talbert, University of North Texas

Table of Contents

1. Introduction

1.1 Hydrogen Storage Challenge

Rapid growth in industry, urbanization, and population has resulted in the increase of greenhouse gas emissions that now risks severe temperature increases in the coming decades. As such, sustainable alternatives to fossil fuels and other emission-producing energy sources have become focuses of global innovation. In the context of this broader energy transition, hydrogen energy has become a central pillar of global decarbonization due to hydrogen's lightness and abundance contributing to its ability to be domestically produced. Additionally, hydrogen-based fuel cells release only water vapor, allowing hydrogen to cut key emissions in carbon-intensive applications where other methods, namely electricity, fail. Hydrogen energy also possesses the key advantage of being able to be produced at any time and regardless of outside conditions, again making it more attractive than intermittent sources of power such as wind and solar [18].

Hydrogen's high current and predicted demand trajectories are fully due to hydrogen's use not only as an energy source, but in the industries of transportation, chemicals, manufacturing, and long-term energy storage. In transportation, hydrogen is especially attractive in the applications of heavy-duty/long distance transport where batteries and other low-emission methods result in concerns regarding weight and charging time [18]. Specifically, a hydrogen fuel-cell vehicle storing 4-10 kilograms of pressurized diatomic hydrogen gas can achieve hundreds of kilometers of range while mimicking the quick refueling capabilities of hydrocarbon-based fuels, only without the carbon emissions [15]. Looking at chemical production, hydrogen is used in the Haber-Bosch process to synthesize ammonia (a key component of commercial fertilizers), aids in the production of methanol, and in the process of hydrodesulfurization, a key component of oil refinery [18], while also serving a prominent role in heavy industries such as steel, ceramics, and glass [16]. Finally, hydrogen gas can be used to store excess energy produced in times of oversupply that can then be stored and utilized later on, addressing the problems related with intermittent forms of renewable energy when it comes to large-scale energy grids [15].

Current hydrogen storage methods, including graphene-based methods, can be generalized into 6 broad categories, the first of which is compressed gas storage. In this method, hydrogen gas is stored at pressures up to 700 bar in specialized containers in order to increase the gas' density as much as possible. While this method only utilizes simple technologies that allow for immediate usage when needed and don't require any advanced processing of the hydrogen, even compressed hydrogen possesses low gravimetric and volumetric energy densities, resulting in the need for large, heavy storage cylinders for any meaningful amount of fuel storage. These storage containers then pose concerns relating to leakage, material fatigue/stress, and the risk of rupture, in addition to the process of compression being extremely energy-intensive [17]. The second simplest form of storage, liquid storage, achieves the maximum energy density of any storage method by cooling the hydrogen to

-253 °C such that the hydrogen condenses into its much-denser liquid form. Liquid hydrogen's energy density and ease of storage compared to gaseous storage makes it ideal for applications such as aerospace travel, but still suffers due to the energy-intensitivity of liquification and the choice between fragile insulative containers and continuous energy losses to boil-off [17]. The third category of storage, cryogenic compression, combines elements of gaseous and liquid storage by subjecting the hydrogen to both high pressures and low temperatures, allowing the increase of energy densities and decrease of boil-off while not requiring extreme conditions. However, it inherits challenges from both parent techniques in that it requires costly, complex materials and systems to handle both low temperatures and high pressures, while still facing safety and container stress concerns [18]. Moving to materials-based hydrogen storage, hydrogen can be adhered to physical materials through either physisorption or chemisorption. Firstly, physisorption involves the storing of hydrogen through the adsorption of hydrogen gas molecules onto the surface of a high surface area substance (ex. metal-organic frameworks, carbon nanotubes, etc.) through Van-der-Waals forces: weak physical forces that allow the hydrogen molecules to adhere without dissociation. Because of this lack of dissociation, physisorption presents the most reversible method of storage through annealing. However, the same weak physical forces that allow ease of hydrogen release make it so that the maintenance of adsorption requires cryogenic conditions that take a similar energy penalty as with other storage forms. Along with the heaviness and cost of these porous, physisorption-compatible materials such as metal-organic frameworks, the trade-offs that physisorption poses make it impractical for any large-scale hydrogen application [18]. Comparatively, chemisorption relies on the chemical bonding of hydrogen to the storage materials, usually metal hydrides or other hydrogen-containing compounds. Strong chemical bonds allow for materials to achieve extremely high energy densities in a compact solid or liquid form at near-ambient pressures and temperatures, alleviating long-term storage concerns. However, these strong chemical bonds make it so that there is a large energy input to release the hydrogen. More importantly, chemisorption faces massive weight efficiency concerns due to the sheer weight of most materials applicable for chemisorption of hydrogen, again limiting materials such as metal hydrides for large-scale application [18].

Chemisorption presents the most practical method of storing hydrogen, only facing drawbacks due to weight and desorption concerns. However, graphene offers a unique, lightweight adsorption material for chemisorptive storage. Graphene can form C-H bonds with adsorbed hydrogen molecules, addressing both the mass and structural concerns that arise from more conventional methods of chemisorption. Rather than compounds containing heavy metals, graphene's composition of a hexagonal lattice of only light carbon molecules allows it to store an extremely large amount of hydrogen for a very little cost in weight. Additionally, graphene's strength as a material adds to its weight efficiency and resistance against strain, only increasing its storage versatility. While the chemical-bonding nature of chemisorption still presents the issue of high-energy hydrogen release, tuning of the C-H bond strength is possible through the modification of graphene. As such, graphene-based hydrogen storage is able to combine the sheer capacity and safety of chemisorptive storage while also the practicality of other methods, proving promising for the material's applications in hydrogen storage and hydrogen's application throughout all industries [15].

Compressed Gas	Liquid	Cryogenic Compression	Physisorption	Conventional Chemisorption	Graphene-Based Chemisorption
• Commonly available and attainable technology • Simple and fast refueling • Relatively low storage cost	• Highest volumetric density • Use in long-term transport • Low pressure storage	• Higher density than pure gas • Less boil-off than liquid	• Easily reversible with fast kinetics • Safer handling in solid-form	• Very high volumetric density • Ambient conditions • Safer due to solid state and strong bonding	• High density without excessive weight • Solid-state safety and low energy and maintenance costs
• Low density • High-energy cost for compression • Safety risks with high pressures	• High energy cost for liquefaction • Boil-off losses or higher maintenance costs • Complex cryogenic storage systems	• Complex hybrid compression and liquefaction system • Costly storage tanks • Added energy costs	• Very low storage capacity • Cryogenic cooling needed (storage + energy costs) • Material packing limits	• Heavy materials reduce gravimetric density • Slow kinetics, high energy to release hydrogen	• Still under development • Performance depends on defect engineering and scalability

Figure 1: Comparison of Hydrogen Storage Technologies. Advantages highlighted in green, drawbacks highlighted in red.

1.2 Graphene as a Hydrogen Storage Vehicle

Graphene is a 2-dimensional material in the fact that it is a one-atom thick sheet of carbons atoms arranged in a hexagonal honeycomb lattice such that each carbon atom is bonded to exactly three others, creating uniform sp^2 hybridization among all atoms. Graphene's structure as a single layer of a light element in a uniform lattice provides it with exceptional properties. Graphene is light, mechanically robust, and most of all, has an extremely large surface area, all of which make it exceptional for hydrogen adsorption. Graphene's surface area allows large hydrogen energy densities, while its physical and chemical stability allows it to endure repeated adsorption and desorption cycles while also leaving room for novel physical storage strategies that further increase its weight efficiency, the main drawback of chemisorption [15]. However, diatomic hydrogen gas cannot bond directly to the carbon atoms in graphene. Rather, when individual hydrogen atoms bond to graphene's structure, they creates defects in which carbon atoms that were once only bonded to three other atoms (sp^2 hybridization) form an extra bond with the hydrogen atom, resulting in a carbon atom that now exhibits sp^3 hybridization, properly named sp^3-type defects.

Hydrogenated graphene has been thoroughly characterized and studied through a variety of different techniques. In Raman spectra, hydrogenated graphene develops a pronounced D-band (~1350 cm^{-1}) and an increased D/G intensity ratio (I_D/I_G), signaling the creation of defects (C–H bonds) that are absent in pristine graphene. These Raman features revert closer to the graphene baseline after dehydrogenation, confirming the reversibility of the sp^3/sp^2 transition.

In addition to methods such as electrochemical reduction, direct deposition, and plasma hydrogenation, it has been suggested that when graphene is exposed to low-energy electron irradiation in the range of 1-30 KeV, bonds in adsorbed H_2O or NH_3 molecules can be broken, resulting in the presence of lone hydrogen atoms that then chemisorb onto the graphene, resulting in hydrogenation without any loss of carbon atoms. This hypothesis of irradiation-induced hydrogenation is supported through a wide range of different characterizations. Graphene that was exposed to polar H-containing molecules when irradiated provided greatly different Raman spectra than untreated samples. Annealing studies have then demonstrated that as the sample is heated to a sufficient

temperature for hydrogen desorption, the irradiation-induced Raman changes reverse, again providing evidence for reversible hydrogenation [5].

1.3 Knowledge Gap and Aim of Study

While the characterization of hydrogenated graphene is extremely comprehensive and promising for the material's applications in hydrogen storage, these characterizations focus primarily on studying pristine graphene flakes, rather than materials derived from graphene that exhibit different properties, namely GO and rGO: graphene oxide and reduced graphene oxide. In these graphene derivatives, oxygen-containing functional groups are bonded to the graphene's lattice, creating sp^3 defects in the same way that hydrogen adsorbates would. While GO has an abundance of these functional groups, rGO has significantly fewer of these absorbents.

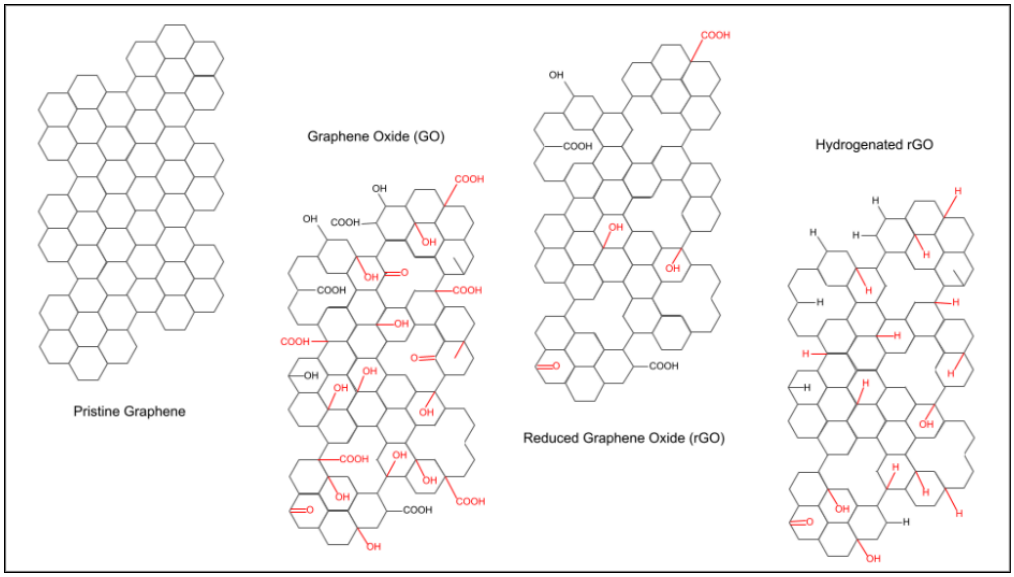

Figure 2: Visual Comparison of Pristine Graphene, Graphene Oxide, Reduced Graphene Oxide, and Hydrogenated Reduced Graphene Oxide. Instances of sp^3 hybridization defects are highlighted in red.

Looking at past studies on GO/rGO, characterizations of fully hydrogenated forms of these materials are scarce, but again primarily emphasize the changes in properties that can occur between pristine graphene and its derivatives. Looking at irradiation studies, irradiation has been conducted on GO/rGO, but only in the extremely high range of 10 MeV. This parameter is significant due to its being much above the 85 KeV threshold for carbon atoms to suffer knock-on damage and other severe disruptions to the lattice. Primarily, this high-energy irradiation of GO and rGO produces two main effects: the removal of oxygen groups via C-O bond scission and crosslink formation between different graphene sheets. Characterizations of the irradiated graphene oxides such as XPS, FTIR, and XRD show irradiation results in net deoxygenation through the removal of sp^3 defects (oxygen-containing functional groups that were previously bonded to the GO) and restoration of sp^2 domains. As these groups are removed, the carbon sheets become less hydrophilic while also incorporating vacancies/interstitials that can be constructed into interlayer bridges that bond different sheets together, leading to crosslinkage [12]. Evidence for 10 MeV-induced cross linkage has been shown through characterizations of mechanical strength and other properties such as conductivity, which indicate that in irradiated rGO, adjacent layers exhibit bonding much stronger than van der Waals contacts [7].

However, the low-energy irradiation of GO/rGO, irradiation that is much less likely to produce massive disruptions in the materials' lattices, has gone largely unstudied. Both confirmed hydrogenation studies and studies that demonstrate the possibility of irradiation-induced hydrogenation have primarily focused on pristine graphene flakes, leaving room for the characterization of rGO under low-energy irradiation.

Reduced graphene oxide also possesses many practical advantages over graphene flakes. In many applications that require non-chemical aspects of graphene, GO or rGO is utilized instead due to their advantages in solubility, size-control, and scalable synthesis. As such, the objective of this study is to further investigate rGO as a possible hydrogen storage vehicle through the process of low-energy electron irradiation. We seek to use Raman spectroscopy to determine if low-energy electrons are still able to induce the restoration of sp^2 domains, similar to the process that occurs with high energy radiation, as well as understanding other possible effects that irradiation can have on rGO that are applicable to the possibility of hydrogen storage. Based on previous results regarding the capabilities of irradiation to further reduce GO/rGO, and its plausibility of inducing hydrogen chemisorption in graphene, the study holds the hypothesis that the low-energy irradiation of rGO will further decrease the samples oxygen content while introducing new sp^3 defects that are possibly hydrogen adsorbates.

2. Literature Review

2.1 Raman Defect Metrics for GO/rGO

Raman spectroscopy, which utilizes the inelastic scattering of photons to characterize the bonds within a chemical sample, is a primary method for characterizing graphene-based materials, due to their properties being heavily altered by what other atoms or molecules are bonded to the carbon lattice. Raman spectra of pristine graphene exhibit three primary first-order peaks: a G-band at 1580 cm^{-1} arising from sp^2 C–C bonds, a D-band at 1350 cm^{-1}, which is a defect-activated peak that appears only in the presence of lattice imperfections (fully pristine graphene shows no D peak), and a D'-band at 1620 cm^{-1} that is also activated by defects [10]. However, the Raman spectra of GO/rGO samples prove to be more nuanced. Because of their extremely high concentration of defects, the D′ contribution is significant in these materials, with its intensity significantly impacting the other peaks. Most prominently, there exists a peak at ~1600 cm-1 that is in fact a superposition of the D' and G peaks [10]. As such, this composite peak is referred to as G_{app}. Understanding and comparing all four of the peaks, whether they are only observed or truly present, is key to understanding the defect composition of a GO/rGO sample.

The peak height ratio I_D/I_G is a common measure of defect density in more pristine graphene, but its reliability breaks down when observing GO or rGO. In low to moderate disorder, I_D/I_G increases with defect density (proportionally to the inverse square of the average distance between defects), but at high levels of disorder, the value becomes non-monotonic against increases in defect density. Ferrari–Robertson's amorphization trajectory explains this: below 2 nm domain size, I_D/I_G increases with increasing order, while above 2 nm it decreases with increasing order. However, even heavily-oxidized GO contains large graphitic domains (areas with little to no functional groups) that cause it to deviate from even this non-monotonic model. Considering that the true G-peak is further convoluted by its overlap with the more sensitive D' band, I_D/I_G is much less reliable than other metrics for assessing defect density.

Aside from the I_D/I_G ratio, the ratio of D to D′ peak intensities $I_D/I_{D'}$ and its integrated area counterpart $A_D/A_{D'}$ are valuable indicators of the type of defects present in a graphene sample. Different defect types (vacancies, boundaries, or sp^3-bonded functional groups such as those in GO) affect the D and D′ bands differently. Because sp^3 defects (such as epoxy or hydroxyl groups in GO) and sp^2 defects (such as vacancies or edges) activate the D and D′ modes to different extents, the $I_D/I_{D'}$ ratio serves to distinguish defect chemistries. GO and rGO, which contain many sp^3-functional defects, tend to exhibit a higher $I_D/I_{D'}$ ratios compared to graphenes with only sp^2 planar defects. In contrast, graphene with mainly sp^2 lattice vacancies shows a lower $I_D/I_{D'}$. Thus, examining the D-to-D′ intensity or area ratio yields inferences regarding whether a given sample's defects are dominated by functional groups (sp^3 character) or by structural imperfections in the lattice. As long as the defect density isn't extremely high such that individual peaks can be identified and computed, these ratios are also independent of overall defect density, furthering their use as indicators of defect type.

King. et al [10] established the use of the difference in peak centers D′ - G_{app} as a method of measuring overall defect density for GO and rGO. The D′ - G_{app} value correlates strongly and monotonically with the sample's oxidation level, as measured by the carbon/oxygen (C/O) atomic ratio. Across many GO and rGO samples, the authors found the trend that larger D′–G_{app} separations correlate with higher C/O ratio (a more reduced, graphitic sample). GO materials with low C/O show a small or even negative D′ - G_{app} , while highly reduced samples (or pristine graphene) exhibit much higher D′ - G_{app} values. This linear correlation makes D′ - G_{app} an excellent metric for the degree of reduction of GO. Unlike I_D/I_G, which varies inconsistently, D′ - G_{app} increases steadily as oxygen functionalities are removed, enabling quantitative assessment of reduction level [10].

Metric	Measured Property	Defect Correlation	Limitations
I_D/I_G	Intensity ratio of D peak to G peak	Tracks defect density, rising in low-defect lattices, then falling at very high disorder, creating a non-monotonic relationship.	Unreliable for GO/rGO due to overlapping of peaks and sustained pristine-like regions, cannot quantify defect density alone.
D' - G_{app}	Wavenumber separation between actual D' and the apparent G peak (G_{app})	Increases monotonically with C/O and sp^2 restoration/oxygen removal. Smallest in GO, larger in rGO, largest in pristine graphene.	Interpretation can become conflicted at extreme disorders as D' and G become more overlapped.
$I_D/I_{D'}$	Intensity ratio of D peak to D' peak	Indicator of defect type, increasing as sp^3 fraction rises. Highest for sp^3-type functionalization , intermediate for vacancies, lowest for grain boundaries.	Absolute thresholds for different defect types in pristine graphene don't translate to GO/rGO.
$A_D/A_{D'}$	Integrated area ratio of D peak to D'	Mirrors $I_D/I_{D'}$ as indicator of defect type, with larger values correlating to greater sp^3 character.	Requires reliable deconvolution, unable to distinguish properties different than those measured by $I_D/I_{D'}$

Figure 3: Chart of Defect Metrics and Structural Meanings

2.2 Electron Irradiation's Effects on GO/rGO

Yang et al. 2019 [11] observed the effects of 1.8 MeV electron irradiation of GO in an aqueous solution, while Jin et al. 2013 [7] characterized rGo papers subjected to a 10 MeV beam at varying dosages. Yang et al. 2019 found that high-energy electron-beam causes radiolysis, generating hydrated electrons that remove oxygen functional groups such as hydroxyl, epoxide, carbonyl, and carboxyl. Additionally, the electron beam induces direct bond scission in GO's carbon lattice, with higher doses leading to more lattice defects and disruption of the sp^2 network [11]. Jin et al. 2013 achieved similar results, with scanning electron microscope (SEM) images

showing irradiation-induced surface damage that grows with dose, consistent with removal of surface carbon atoms. Additionally, various simulations support a bond-scission dominated mechanism [7].

XPS and FTIR analysis from both groups support the removal of oxygen groups via C-O bond breaking. XPS reveals shows a sharp increase in the C/O ratio (1.6 to 4.8) and decrease of oxygen-containing groups such as epoxy/alkoxy (39% to 11%), hydroxyl (42% to 26%), and carboxyl (20% to 12%) along with consequent decreases in the bonds of these groups with carbon molecules [11]. Similarly, C-H and C-O bond percentages steeply decrease with dosage [7].

Yang et al. 2019's results suggest the possibility of cross-linking between adjacent GO sheets due to the fact that as oxygen groups are removed, rGO sheets become less hydrophilic and tend to agglomerate under irradiation. Additionally, high-energy electrons may generate carbon radicals on the sheets, which could recombine into new C–C bonds between different sheets [11]. Jin et al. 2013 then shows evidence of high energy irradiation-induced cross linkage through measurements of mechanical resistance and electrical conductivity that indicates stronger bonding than possible with van der Waals forces [7].

2.3 Prior Hydrogenation Studies

Elias et al. 2009 [6] demonstrates the reversible, definitive hydrogenation of single-layer graphene flakes by exposing pristine flakes to a hydrogen/argon plasma. Subsequent Raman spectroscopy was able to show C–H bond-driven sp^3 conversion. A sharp D peak and D′ emerge, with the particularly prominent D peak contributing to an increased $I_D/I_{D'}$ ratio indicative of increased sp^3 defect type. Additionally, the study demonstrates the reversibility of this hydrogen through annealing at temperatures greater than 400°C, which resulted in the collapse of defect peaks. Additionally, free-standing graphene membranes hydrogenated more easily than supported flakes because both sides were accessible [6]. Looking at rGO, these flake-level results prove the core mechanism of reversible sp^2 to sp^3 conversion via C–H chemisorption, exactly what is needed for hydrogen storage. They imply that rGO powders/films (with higher surface area and abundant edge/defect sites) are able to be easily hydrogenated. Reduced graphene oxide powder also incorporates the advantage of the maximization of two-sided exposure, while still being able to be characterized by Raman spectroscopy [6]. Tozzini et al. 2013 [15] further explores the possibilities and characterization of hydrogenated graphene, emphasizing that the removal of oxygen functionalities further improve hydrogen accessibility on the graphene's lattice, pointing to rGO as a scalable candidate for hydrogen storage [15].

Looking at the possibility of irradiation-induced hydrogenation, the Perez group has made substantial progress in terms of providing evidence of hydrogenation for electron-irradiated graphene flakes. Specifically, Ojo et al. 2023 [5] observed that after irradiation, suspended monolayer regions of graphene exhibited a D-to-G intensity ratio I_D/I_G up to 6.3, far above the 3.3 maximum typically seen for vacancy-type damage in supported graphene. The elevated I_D/I_G implies a different defect type, consistent with dense sp^3 defects rather than just vacancies. $I_D/I_{D'}$ further signifies the addition of sp^3 defects, with its value of 9 being in the range expected for sp^3-type defects (adsorbates), whereas vacancies give lower ratios of 5-7. Thermal annealing of the irradiated samples results in reversals of these changes, again pointing to desorption. Next, further annealing data yields activation energies that align with hydrogen chemical processes, again indicating that hydrogenation is the dominant process. Ojo et al. suggests that this hydrogenation is due to the trapping of air and moisture under the

membrane as the graphene is mechanically exfoliated in ambient conditions. Water molecules then would then have formed thin hydrogen-bonded layers on the suspended graphene surface, providing a large amount of H_2O that can interact under the beam. Then, the irradiation induced breaking of H-OH bonds would result in the release of atomic hydrogen that then chemisorbs onto the graphene's surface, similar to supporting studies in which exposure to other polar hydrogen-containing molecules gave results suggesting hydrogenation, while exposure to inert molecules had no effect. Additionally, graphene's physical properties seal the hole such that the drum retains almost all the ambient gas inside. After an hour in vacuum, the internal pressure only slightly decreased to 0.96 atm (from its initial 1 atm), meaning that a substantial amount of water vapor and hydrogen remained trapped during irradiation and was able to fuel the process of irradiation-induced chemisorption.

2.4 Industrial Implications of hydrogenated rGO Powder

Regarding the increased practicality of rGO powder compared to graphene flakes, Tozzini et al. 2012 [15] notes that current exfoliation and reduction methods can yield rGO powders in high concentrations of several mg/mL. Powders therefore form a practical source for producing membranes, coatings, or composite materials tailored to storage systems. Additionally, compared with pristine single-layer graphene sheets, which are challenging to prepare in bulk, the powder state makes rGO powder much more attractive for bulk applications and realistic for scaling up to industrially relevant hydrogen storage systems [15]. Morse et al. 2021 [14] adds that hydrogenated powders retain their hydrogen content even after being processed into compressed pellets, furthering the possibility for large scale systems.

3. Materials and Methods

3.1 Sample Preparation

Reduced graphene oxide powder was purchased from Graphenea, with the following specifications. The powder was chemically reduced, meaning that it was treated with a reducing agent that was able to remove oxygen-containing functional groups and restore the sp^2 structure. For particle size, 90% of the particles were below 10-15 μm, 50% were below 4-6 μm, and 10% were below 1-3 μm. By TGA, the humidity was measured at 3.7-4.2%. It had an electrical conductivity of 667 S/m, a specific surface area of 423 – 498 m^2/g and an apparent density of 0.20-0.30 g/cm^3. Elemental analysis showed that the elemental composition of the powder is as follows: C (80-87%), O (13 – 17%), H (0-1%), N (0-1%), S (0-1%). Preparation of the film was done through thoroughly combining a sample of powder with deionised water in a mortar and pestle to create a homogenous film. In addition to the water itself hydrating the rGO, this process was conducted in ambient temperature and pressure to recreate conditions in which water-vapor was able to form a thin-hydrogen bonded layer on the rGO that is able to interact with the electron beam. After proper preparation, the film was deposited onto a 1.5 cm by 1.5 cm (2.25 cm^2) wafer of SiO_2 and let to air dry. As with before, all processes were performed in ambient pressures and temperatures, as well as the samples being consistently exposed to air in order to give it ample opportunity to naturally hydrate.

3.2 Electron Irradiation

The beam parameters were set up as follows: electrons were baked off of a tungsten filament and accelerated to an energy of 1.5 KeV, and collided with the sample such that the sample received a current of 2 nA. After 2 hours of irradiation, the sample received a total dosage of 3×10^{16} electrons/cm². The sample was irradiated in ultra-high-vacuum conditions, with a base pressure of 10^{-10} - 10^{-12} torr significant for reducing contamination from sources other than the intentional deposition of water vapor. The total dosage of 3×10^{16} electrons/cm² was distributed uniformly over the sample through a continuous manual scanning of the beam across the sample throughout the process of irradiation.

3.3 Raman Spectroscopy

The Raman instrument used was the Renishaw inVia InSpect confocal Raman microscope with the following acquisition parameters: laser excitation wavelength of 532 nm, grating of 1800 l/mm, laser power 10% (maximum power is 50 mW, meaning that 10% power is 5 mW), and 100x objective. All collected spectra had a center of 1800 cm^{-1}, with the x-axis being bounded from 934.3 cm^{-1} to 2548.41 cm^{-1}. All Raman spectra were acquired with an exposure time of 10 seconds and 4 accumulations that were then averaged in order to reduce the signal-to-noise ratio.

After acquisition, Raman spectra were deconvolved into Voigt peaks, namely a D, G, and D' peak, the combination of the three giving the consistently most accurate curve fits. After allowing the curve to fit and the peaks to be manipulated such that they matched the spectra, peaks were analyzed and areas, centers, and heights were recorded. Computed metrics then consisted of $I_D/I_{D'}$, $A_D/A_{D'}$, and D′ - G_{app}, in order to yield results that could unambiguously and directly provide insight as to irradiation's effect on the rGO film. In order to compute the value of G_{app}, a separate deconvolution was conducted in addition to main deconvolution into D, G, and D' peaks, in which the spectra were only deconvolved into a D and G_{app} such that the value of G_{app} could be recorded and used along with the main deconvolution to calculate D' - G_{app}.

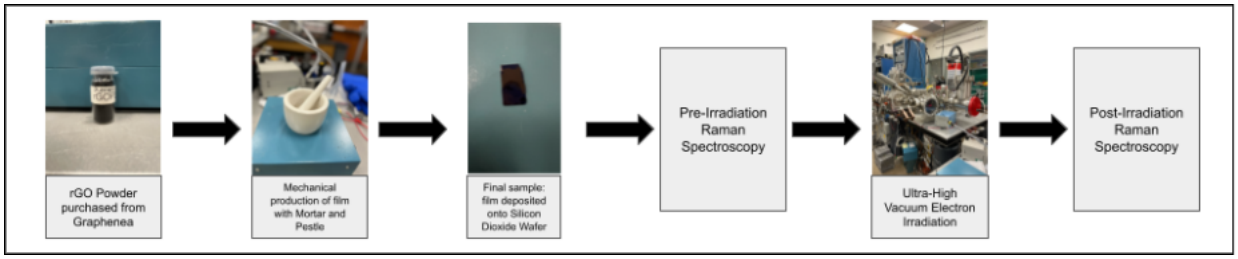

Figure 4: Schematic of Experimental Process

4. Results

4.1 Deconvolved Raman Spectra Before and After Irradiation

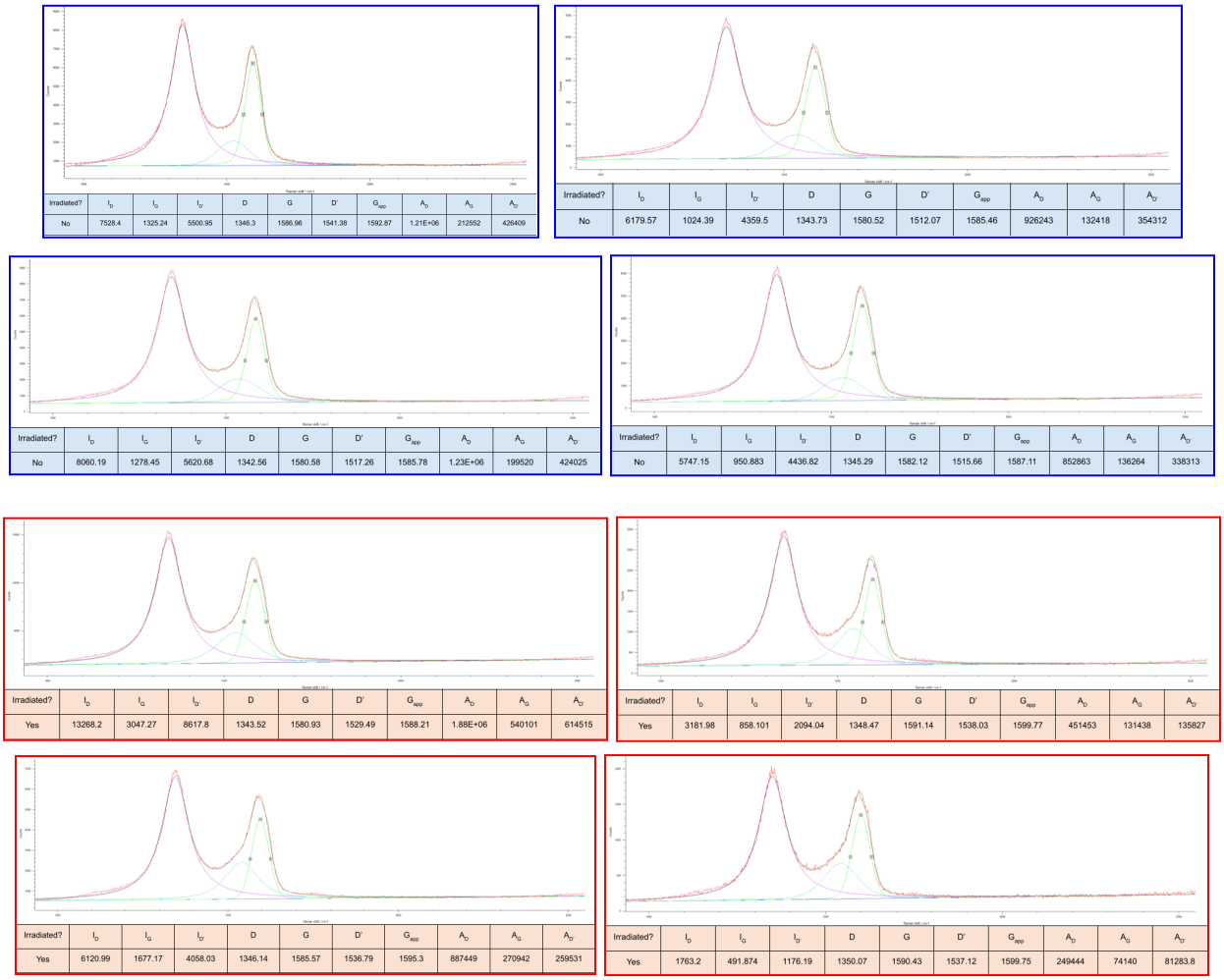

Irradiated?	I_D	I_G	$I_{D'}$	D	G	D'	G_{app}	A_D	A_G	$A_{D'}$
No	7528.4	1325.24	5500.95	1346.3	1586.96	1541.38	1592.87	1.21E+06	212552	426409

Irradiated?	I_D	I_G	$I_{D'}$	D	G	D'	G_{app}	A_D	A_G	$A_{D'}$
No	6179.57	1024.39	4359.5	1343.73	1580.52	1512.07	1585.46	926243	132418	354312

Irradiated?	I_D	I_G	$I_{D'}$	D	G	D'	G_{app}	A_D	A_G	$A_{D'}$
No	8060.19	1278.45	5620.68	1342.56	1580.58	1517.26	1585.78	1.23E+06	199520	424025

Irradiated?	I_D	I_G	$I_{D'}$	D	G	D'	G_{app}	A_D	A_G	$A_{D'}$
No	5747.15	950.883	4436.82	1345.29	1582.12	1515.66	1587.11	852863	136264	338313

Irradiated?	I_D	I_G	$I_{D'}$	D	G	D'	G_{app}	A_D	A_G	$A_{D'}$
Yes	13268.2	3047.27	8617.8	1343.52	1580.93	1529.49	1588.21	1.88E+06	540101	614515

Irradiated?	I_D	I_G	$I_{D'}$	D	G	D'	G_{app}	A_D	A_G	$A_{D'}$
Yes	3181.98	858.101	2094.04	1348.47	1591.14	1538.03	1599.77	451453	131438	135827

Irradiated?	I_D	I_G	$I_{D'}$	D	G	D'	G_{app}	A_D	A_G	$A_{D'}$
Yes	6120.99	1677.17	4058.03	1346.14	1585.57	1536.79	1595.3	887449	270942	259531

Irradiated?	I_D	I_G	$I_{D'}$	D	G	D'	G_{app}	A_D	A_G	$A_{D'}$
Yes	1763.2	491.874	1176.19	1350.07	1590.43	1537.12	1599.75	249444	74140	81283.8

Figures 5-13: Raw Raman Spectra and Component Peaks, with Parameters. Spectra highlighted in blue are for samples pre-irradiation, and spectra highlighted in red were acquired post-irradiation.

4.2 Quantitative Metrics

Point	Irradiated?	D' - G_{app}	$I_D/I_{D'}$	$A_D/A_{D'}$
1	Yes	5.91	1.368563612	2.844499061
2	Yes	4.94	1.417495126	2.614201608
3	Yes	5.2	1.434023997	2.901692117
4	Yes	4.99	1.29533089	2.520928844
5	No	7.28	1.539627283	3.063733188
6	No	8.63	1.519541174	3.32373534
7	No	9.73	1.508364896	3.419433517
8	No	9.32	1.49907753	3.068803378

5. Discussion

5.1 Evidence for Oxygen Removal

The Raman data shows that the 1.5 KeV irradiation significantly increased the D′ - G_{app} center separation in the rGO film, rising from 4.9–5.9 cm^{-1} in non-irradiated samples to 7.3 - 9.7 cm^{-1} after irradiation. The D′ - G_{app} metric is strongly correlated with the degree of oxygen removal: as C–O bonds are cleaved, the G band upshifts and the D′ band becomes more distinct, widening the gap between them. All observed values for D' - G_{app} fall within the range of 0 to 25 cm^{-1} that classifies them as rGO (as expected), but the irradiated samples moved closer to crossing the 25 cm^{-1} threshold to be classified as pristine graphene, demonstrating the possible reduction caused by the irradiation. This observed widening of D′ - G_{app} is best explained by irradiation-induced radiolysis of oxygen-containing groups. Their removal restores sp^2 domains in the lattice, yielding the observed shifts in center difference D' - G_{app}.

These results are consistent with the previously-observed scission of C-O bonds caused by irradiation. XPS analysis, FTIR spectra, and UV-vis evidence all demonstrate that irradiation causes C/O ratios to climb as oxygen-containing functional groups are no longer bonded to the lattice. The convergence of the observed increase in D' - G_{app} with these previous reports strengthens the case that electron beam irradiation further reduced rGO film.

5.2 Evidence for sp^3-Type Defect Shift

Irradiation produced a measurable increase in $I_D/I_{D'}$. In the non-irradiated samples, $I_D/I_{D'}$ values clustered tightly around 1.30-1.43, while the irradiated samples rose to 1.50-1.54. Though the increase is low, its consistency across all acquired spectra represents an experimentally observed shift. Within the Raman framework for graphene and its derivatives, increases in $I_D/I_{D'}$ are linked to increases in sp^3 defects compared to other defect types such as vacancies or edge-disorders. As such, even the fractional rise in $I_D/I_{D'}$ suggests that irradiation induced sp^3 defects (adsorbates) were introduced into the rGO's lattice.

This is further corroborated by the uniform increase in $A_D/A_{D'}$ observed after irradiation. While intensities may be subject to noise captured during acquisition, the areas of peaks capture the overall contribution of each peak, and the consistent upward shift in this area ratio strengthens the conclusion of irradiation inducing sp^3 defects. The combined rise in intensity and area-based metrics indicates the validity of the observed effect.

5.3 Possible Hydrogen Adsorption

The simultaneous increases in D' - G_{app}, $I_D/I_{D'}$, and $A_D/A_{D'}$ initially seem contradictory, but when combined yield evidence that irradiation introduces hydrogen defects onto the rGO's structure. The increase in D' - G_{app}

values (indicating a loss of oxygen groups) should be observed along with decreases in $I_D/I_{D'}$ and $A_D/A_{D'}$ due to the restoration of an sp^2 structure, but instead comes with increases in both metrics. This dissonance can be resolved through the conclusion that irradiation does result in the cleavage of C-O bonds and the removal of functional groups, but also induces the adsorption of a different type of functional group. In particular, the creation of additional sp^3 signatures alongside oxygen removal suggests that irradiation enables chemisorption of new species, most plausibly hydrogen atoms derived from water introduced to the graphene through the film and ambient conditions. Thus, the dual trends in Raman metrics present complementary evidence that electron irradiation drives a two-step process: deoxygenation of rGO accompanied by the introduction of sp^3 defects that may correspond to hydrogen adsorption, therefore mirroring the study's original hypothesis regarding the effect of irradiation on rGO.

6. Limitations and Future Work

6.1 Limitations

This prediction of irradiation-induced hydrogenation is limited by Raman spectroscopy's inability to directly confirm the identity of adsorbates. While metrics such as D' - G_{app}, $I_D/I_{D'}$, and $A_D/A_{D'}$ can provide insight as to the properties of defects and other aspects of the rGO's structure, direct identification of adsorbates requires additional analysis.

As such, the current level of data is unable to distinguish hydrogen adsorption from other sources of sp^3 defects, namely cross linking. While cross linking and the removal of carbon atoms from the lattice are other possible explanations for the observed results, it's important to distinguish the low-energy nature of the current results. While cross linkage and knock-on damage were observed at energies around 10 MeV, the 1.5 KeV irradiation that samples experienced in this study carried far less potential for damage than the 85 KeV knock-on threshold that is responsible for the removal of carbon atoms and crosslink formation. As such, adsorption (possibly hydrogen atoms) is the most plausible explanation for the observed effects.

6.2 Hydrogen Confirmation

A variety of routes can be taken in order to concretely confirm the identity of adsorbates on the rGO film. The basis of annealing-based desorption lies in the property that at temperatures greater than 400°C, hydrogenated graphene undergoes thermal decomposition and releases H_2 gas. This hydrogen release is parameterized by temperature and heating time, with ideal decomposition occurring in nitrogen, hydrogen, or vacuum environments [14]. As such, in order to provide confirmation of hydrogen adsorbates, irradiated samples could be heated in ideal conditions, along with the subsequent performing of thermogravimetric analysis or mass spectrometry. Both methods would provide insight as to the mass of adsorbates released from the film, which could then be compared with known values of masses for hydrogen-based adsorbates to provide evidence of hydrogen adsorption.

Additionally, to provide further evidence of hydrogenation, hydrogen atoms can be unambiguously deposited on the film through the cracking of hydrogen gas into two hydrogen atoms, achieved through the heating of a tungsten filament. The level of hydrogenation is tunable through filament current and resulting temperature, and measurable through the use of a complementary platinum detector to induce the recombination of hydrogen atoms into H_2, whose temperature change is able to reveal the level of hydrogenation. Different levels of hydrogenated film could undergo the same characterization process as different levels of irradiated graphene, helping to provide direct evidence for the plausibility of irradiation-induced hydrogenation of reduced graphene oxide powder.

7. References

[1] A. Tararan, A. Zobelli, A. M. Benito, W. K. Maser, and Odile Stéphan, Revisiting Graphene Oxide Chemistry via Spatially-Resolved Electron Energy Loss Spectroscopy, Chemistry of Materials 28, 3741 (2016).

[2] Atsushi Sutoh, Y. Okada, S. Ohta, and M. Kawabe, Cracking Efficiency of Hydrogen with Tungsten Filament in Molecular Beam Epitaxy, Japanese Journal of Applied Physics 34, (1995).

[3] A. Eckmann, A. Felten, Artem Mishchenko, L. Britnell, R. Krupke, K. S. Novoselov, and Cinzia Casiraghi, Probing the Nature of Defects in Graphene by Raman Spectroscopy, Nano Letters 12, 3925 (2012).

[4] A. Augusto, Santos, Filipe, Odilon Souza Leite-Barbosa, L. Altoé, and Junior, Chemical and Structural Analysis of Graphene Oxide Reduced with Naringenin: A Natural Product-Based Alternative, Journal of Materials Research and Technology (2025).

[5] I. Ojo, E. Hathaway, J. Li, R. Gonzalez, Y. Jiang, J. Cui, and J. Perez, Effects of Electron Irradiation on Graphene Drums, Journal of Vacuum Science & Technology a Vacuum Surfaces and Films 42, (2023).

[6] D. C. Elias et al., Control of Graphene's Properties by Reversible Hydrogenation: Evidence for Graphane, Science 323, 610 (2009).

[7] E. Jin, J. He, K. Sheng, Z. Zhang, G. Shi, and Q. Zheng, Electron-Irradiation-Induced Reinforcement of Reduced Graphene Oxide Papers, Acta Materialia 61, 6466 (2013).

[8] L. Chen, Z. Xu, J. Li, C. Min, L. Liu, X. Song, G. Chen, and X. Meng, Reduction and Disorder in Graphene Oxide Induced by Electron-Beam Irradiation, Materials Letters 65, 1229 (2011).

[9] R. Muzyka, S. Drewniak, Tadeusz Pustelny, Maciej Chrubasik, and Grażyna Gryglewicz, Characterization of Graphite Oxide and Reduced Graphene Oxide Obtained from Different Graphite Precursors and Oxidized by Different Methods Using Raman Spectroscopy, Materials 11, 1050 (2018).

[10] A. A. K. King, B. R. Davies, N. Noorbehesht, P. Newman, T. L. Church, A. T. Harris, J. M. Razal, and A. I. Minett, A New Raman Metric for the Characterisation of Graphene Oxide and Its Derivatives, Scientific Reports 6, (2016).

[11] Y. Yang, L. Chen, D.-Y. Li, R.-B. Yi, J.-W. Mo, M.-H. Wu, and G. Xu, Controllable Reduction of Graphene Oxide by Electron-Beam Irradiation, RSC Advances 9, 3597 (2019).

[12] H. Zare, M. A. Hosseini, and Shahryar Malekie, Evaluation of 10 MeV Electron Irradiation-Induced Defects in Graphene Oxide and Multi-Walled Carbon Nanotube Using a Multi-Analytical Approach, Nuclear Instruments and Methods in Physics Research Section B Beam Interactions with Materials and Atoms 543, 165089 (2023).

[13] Y. Fei, S. Fang, and Y. H. Hu, Synthesis, Properties and Potential Applications of Hydrogenated Graphene, Chemical Engineering Journal 397, 125408 (2020).

[14] J. R. Morse, D. A. Zugell, E. Patterson, J. W. Baldwin, and H. D. Willauer, Hydrogenated Graphene: Important Material Properties Regarding Its Application for Hydrogen Storage, Journal of Power Sources 494, 229734 (2021).

[15] V. Tozzini and V. Pellegrini, Prospects for Hydrogen Storage in Graphene, Phys. Chem. Chem. Phys. 15, 80 (2013).

[16] A.-M. Chirosca, E. Rusu, and V. Minzu, Green Hydrogen—Production and Storage Methods: Current Status and Future Directions, Energies 17, 5820 (2024).

[17] A. S. Mekonnin, K. Wacławiak, M. Humayun, S. Zhang, and H. Ullah, Hydrogen Storage Technology, and Its Challenges: A Review, Catalysts 15, 260 (2025).

[18] M. Hossain and Z. Siddique, Hydrogen as an Alternative Fuel: A Comprehensive Review of Challenges and Opportunities in Production, Storage, and Transportation, International Journal of Hydrogen Energy 102, 1026 (2025).

[19] W. Liu and G. Speranza, Tuning the Oxygen Content of Reduced Graphene Oxide and Effects on Its Properties, ACS Omega 6, 6195 (2021).

[20] S Bidmeshkipour, M Alidoosti, A. Hosseinzadeh, S M S Seyyedi, M. Elahi, M Pourfath, and S Mohajerzadeh, Hydrogenated Graphene Oxide (H-G-SiO2) Janus Structure: Experimental and Computational Study of Strong Piezo-Electricity Response, Journal of Physics D Applied Physics 53, 175303 (2020).

8. Statement on Outside Assistance

Researchers Name: Avin Gupta

Title of Paper: Electron Irradiation and Raman Characterization of Reduced Graphene Oxide Film

What steps led you to formulate your hypothesis? (Where did you get the idea for your research?) Please be specific: This experiment's hypothesis was formed as a result of discussions with the lab's overseeing professor, Dr. Jose Perez, regarding his group's previous work regarding the electron irradiation of graphene and the plausibility of irradiation-induced hydrogen adsorption onto graphene. After discussing the implications of hydrogenated graphene, the idea to extend the research on graphene flakes to reduced graphene oxide powder came about as a solution to make the results of the lab industrially feasible.

Where did you conduct the major part of your work? (i.e. home, school, or other institutional setting, university lab, medical center, etc.): The majority of research was conducted at the University of North Texas, specifically in the lab of Dr. Jose Perez.

If you worked in an institutional setting, did you work on your project as part of a team or group? If so, how large was the team and who was on the team (students, adult researchers, etc.)? Describe your role on the team: I worked on my project with the assistance of the Perez group, consisting of myself, Dr. Perez, and a team of graduate students. Within this experiment, I served as the head investigator and lead regarding experiment planning and data collection, while utilizing the help of the rest of the team for pure sample construction and data collection.

Describe what parts of the research you did on your own and what parts you received help (i.e. literature search, hypothesis, experimental design, use of special equipment, gathering data, evaluation of data, statistical analysis, conclusions, and preparation of written report (abstract and/or paper): Throughout the process of this experiment, I served as the primary conductor of literature review, hypothesis construction, experimental design, evaluation of data, formation of conclusions, and preparation of a written report. I received assistance from the lab's graduate students with pure lab work such as sample construction, use of special equipment (namely UHV irradiation and Raman Spectroscopy).

Is your research current or a continuation of previous research? If a continuation, please describe the current work and advancement(s) of this research in comparison to the prior work and results: This research is meant to serve as a continuation of the previous research conducted by the Perez group at the University of North Texas. The Perez group performs research mainly regarding the irradiation of two-dimensional materials such as graphene, with the primary goal being to collect evidence that graphene can be hydrogenated through electron-irradiation for hydrogen storage purposes. However, the lab's current work aside from this experiment analyzes pristine graphene flakes. As such, this study is meant to apply the group's previous findings to the more industrially significant material of rGO powder such that the findings regarding hydrogenation are more applicable in an industrial, tangible context. This experiment provides evidence that the groups' previous hypotheses regarding the irradiation-induced hydrogenation of pristine graphene flakes can also be applied to rGO powder.